Vol.4, No.7, Page 2424- 2435, 2026 https://doi.org/10.59628/jast.v4i7.3263 ISSN 2958-9568 JAST

SUN PUBLISHER

مجلة جامعة صنعاء للعلوم التطبيقية والتكنولوجيا

Sana'a University Journal of Applied Sciences and Technology

https://journals.su.edu.ye/index.php/jast/

Propagation Characteristics of Partially Coherent Pin-Like Vortex Beams in Turbulent Biological tissues

Wafa'a A.Al-Bahry , Hassan T. Al-Ahsab , Mohammed S. Qusailah[1] and Abdu A. Alkelly *

Department of Physics, Faculty of Sciences, Sana'a University, Sana'a, Yemen

*Corresponding author: a.alkelly@su.edu.ye

Abstract

This study examined the propagation characteristics of partially coherent pin-like optical (PCPO) vortex beams carrying orbital angular momentum (OAM) within turbulent biological tissues. The objective of this study was to assess the potential of these nanoparticles for deep-tissue optical communication and imaging. By incorporating the biological tissue turbulence spectrum into the analytical framework, we extended the established analytical expressions that describe the evolution of the OAM mode spectrum, spiral spectrum, and channel capacity of PCPO beams in inhomogeneous biological media, which were modeled using fractal-based turbulence power spectra. Numerical simulations were conducted for several representative tissues, including the upper dermis, deep dermis, liver parenchyma, and intestinal epithelium, to assess the impact of tissue heterogeneity parameters, spatial coherence length, and topological charge on beam stability. The findings indicate that the probability of OAM detection diminishes with propagation distance and increasing topological charge, whereas a greater spatial coherence length and larger characteristic heterogeneity length enhance the channel capacity. Biological tissues with higher fractal dimensions and lower correlation lengths exhibit more pronounced turbulence-induced degradation. When the coherence length exceeds approximately 10 μm, the detection probability becomes nearly invariant with distance, suggesting a regime of enhanced robustness. These results provide quantitative insights into the feasibility and limitations of employing partially coherent OAM beams for optical information transfer in biological tissues and offer theoretical guidance for designing OAM-based biomedical photonic systems.

Article Info

Keywords:
Pin-like optical, Vortex beams, Orbital angular momentum, Biological tissues.

Article History:
Received: 25-May-2026,
Revised: 21-June-2026,
Accepted: 04-July-2026,
Published: 28 July 2026.

1. INTRODUCTION

Optical vortex beams, distinguished by their helical wavefronts and well-defined orbital angular momentum (OAM), have garnered increasing interest for applications in optical communication, imaging, micromanipulation, and information encoding [1–5]. Their distinctive phase structure facilitates the multiplexing of OAM modes, thereby offering high-capacity communication channels and enhanced spatial resolution in optical systems[1, 6, 7]. Recently, the propagation of vortex beams in complex scattering environments, such as atmospheric turbulence and random media, has become a focal point of research owing to the significant distortions caused by refractive-index fluctuations[8–10]. Concurrently, biological tissues are increasingly recognized as highly inhomogeneous, weakly turbulent optical media, where internal microstructures, including variations in the refractive index, heterogeneity, and fractal geometry, substantially disrupt coherent beams[11–13]. These refractive-index fluctuations originate from cellular organization, extracellular structures, and dynamic biological processes, rendering biological tissues a challenging yet pertinent environment for optical beam propagation studies[14]. Understanding the performance of structured light in such media is crucial for advancing deep-tissue imaging, optical sensing, and biomedical photonic communica-

©2026 The Author(s). This article is licensed under CC By 4.0

tion systems[15, 16]. Previous studies have explored the behavior of vortex and partially coherent beams in random or turbulent media, including oceanic turbulence, atmospheric channels, and weak biological scattering models[1, 17–19].

However, most prior research has focused either on fully coherent vortex beams or on classical partially coherent sources. Moreover, biological tissues exhibit unique turbulence characteristics, such as short correlation lengths, strong scattering coefficients, and fractal heterogeneity, which differ significantly from the atmospheric or oceanic turbulence models typically employed in OAM research[20]. This gap is even more pronounced given the growing interest in OAM-enabled biomedical imaging, deep-tissue communication, and optical diagnostic systems. Research on the propagation characteristics of partially coherent pin-like vortex beams has primarily focused on atmospheric and oceanic turbulence, with limited studies on their behavior in biological tissues. Biological tissues have unique refractive index fluctuations and scattering mechanisms that can affect coherence, beam confinement, and stability. This study aims to extend the analysis of these beams to turbulent biological environments, offering insights into their behavior under conditions relevant to biological optics by theoretically examining how tissue-induced fluctuations impact their spatial and coherence properties. To the best of our knowledge, no prior study has systematically analyzed the propagation characteristics, OAM mode evolution, and channel capacity of partially coherent pin-like optical (PCPO) vortex beams in turbulent biological tissue. This represents a critical gap in the literature, and addressing it is essential for advancing OAM-based photonic techniques in clinical and biological environments. In this study, we extended the established analytical formulations for the channel capacity, detection probability, and spatial spectrum to investigate the OAM probability density and propagation characteristics of partially coherent pin-like vortex beams in turbulent biological tissues. The focus is on applying these formulations to a biological-tissue turbulence model. By employing the OAM probability density diffraction integral and incorporating a realistic refractive index fluctuation model for biological media, we investigated how spatial coherence, topological charge, tissue fractal dimension, heterogeneity length, and turbulence strength influence beam stability. Numerical simulations of several representative tissues, including the upper dermis, deep dermis, liver parenchyma, and intestinal epithelium, provide new physical insights into the feasibility and limitations of using OAM beams for optical communication and sensing in biological environments.

2. THEORETICAL FRAMEWORK OF PCPO VORTEX BEAMS IN TURBULENT BIOLOGICAL TISSUES

At a distance z in free space, the complex amplitude of PO vortex beams can be expressed as[21]

$$E_{free}(\boldsymbol{r},z) = i^{-|n_0|}\sqrt{\frac{2\pi k}{2-\gamma}}\,\zeta\left[\rho(z)\right]\,J_{n_0}\left[k\,r\,(\delta\,\gamma\,z^{\gamma-1})^{\frac{1}{2-\gamma}}\right] \times(\delta\,\gamma\,z^{\frac{\gamma}{2}})^{\frac{1}{2-\gamma}}\exp\left\{\,i\left[\,\frac{kr^2}{2z}+\frac{k(\gamma-2)}{2\gamma}(\delta^2\gamma^2z^{\gamma})^{\frac{1}{2-\gamma}} -\frac{\pi}{4}(1+2|n_0|)-n_0\,\theta\,\right]\right\}, \quad (1)$$

with

$$\zeta\left[\rho(z)\right] = 3.23\sqrt{\frac{I\left[\rho(z)^{2-\gamma}/(\delta\gamma)\right]}{I_0}}\,i^{|n_0|}\rho(z)^{-\gamma/2} \times\sqrt{\frac{2-\gamma}{2\pi k\gamma\delta}}. \quad (2)$$

where $\boldsymbol{r}=(r,\theta)$ with the radial position in the source plane and θ is the azimuthal angle, $k=\frac{2\pi}{\lambda}$ is the wave number with wavelength λ, $J_{n_0}(x)$ denotes the Bessel function of the first kind of order n_0 that represents the topological charge, γ refers to the phase modulation power, ranging from 0 to 2, n_0 denotes the orbital angular momentum (OAM) mode number, $\zeta[\rho(z)]$ is the initial amplitude modulation function, $\rho(z)=\left(\delta\,\gamma\,z\right)^{\frac{1}{2-\gamma}}$ where $\delta=\frac{C_\rho}{\omega_\rho^\gamma}$ and C_ρ is defined as the phase scaling parameter, which is not restricted to a specific value, and ω_ρ is the phase normalization factor. For the steady state, the analytic peak intensity function $I(z)=I_0$.

Consequently, for the steady state, the analytic peak intensity function $I(z)=I_0$. where r represents the radial position in the source plane, and θ is the azimuthal angle. $k=\frac{2\pi}{\lambda}$ is the wave number, where λ is the wavelength, $J_n(x)$ denotes the Bessel function of the first kind of order $n.n_0$ denotes the orbital angular momentum (OAM) mode number, γ is the phase modulation power, ranging from 0 to 2. Since Eq. Eq. (1) governs the radial field distribution and, in turn, the degree of spatial localization, it is easy to understand how the beam characteristics depend on the parameter γ . A stronger field confinement and a more localized pin-like intensity profile result from smaller values of γ. However, an increase in γ broadens the effective transverse distribution and encourages propagation characteristics similar to Bessel-type beams, such as enhanced reconstruction (self-healing) capability and improved resistance to diffraction [12]. Furthermore, $\zeta[\rho(z)]$ is the initial amplitude modulation function, $\rho(z)=\left(\delta\,\gamma\,z\right)^{\frac{1}{2-\gamma}}$, $\delta=\frac{C_\rho}{\omega_\rho^\gamma}$, C_ρ is defined as the phase-scaling parameter, which is not restricted to a specific value, and ω_ρ is the phase normalization factor[21].

According to the Rytov approximation, the complex amplitude of PCPO vortex beams after propagating a distance z through biological media can be described

©2026 The Author(s). This article is licensed under CC By 4.0

as[17]

$$E(\boldsymbol{r},z) = E_{free}(\boldsymbol{r},z)\,\exp\big[i\,\psi(\boldsymbol{r}) + \psi(\boldsymbol{r},z)\big], \tag{3}$$

where $\psi(\boldsymbol{r})$ accounts for the stochastic phase modulation from the phase diffuser, and $\psi(\boldsymbol{r},z)$ models the complex random phase perturbation arising from biological tissues as the wave propagates. Assuming that the statistics of the biological tissue medium and the partially coherent source are uncorrelated, the second-order cross-spectral density function of PCPO vortex beams can be written as[17]

$$\begin{aligned} W(\boldsymbol{r},\boldsymbol{r}',z) &= \big\langle E(\boldsymbol{r},z)\,E^*(\boldsymbol{r}',z)\big\rangle_{TS} \\ &= E_{free}(\boldsymbol{r},z)\,E^*_{free}(\boldsymbol{r}',z) \\ &\quad\times\big\langle\exp\big[i\,\psi(\boldsymbol{r},z) + \psi^*(\boldsymbol{r}',z)\big]\big\rangle_T \\ &\quad\times\mu(\boldsymbol{r},\boldsymbol{r}'). \end{aligned} \tag{4}$$

where $\boldsymbol{r}' = (r,\theta')$ is the transverse coordinate in polar form, and $\mu(\boldsymbol{r},\boldsymbol{r}')$ denotes the spatial coherence function (or spectral degree of coherence) at the source plane given by [18]

$$\begin{aligned} \mu(r,r') &= \langle\exp[i\,\psi(r) - i\,\psi(r')]\rangle_S \\ &= \exp\left[-\frac{2r^2 - 2r^2\cos(\theta-\theta')}{\rho_s^2}\right]. \end{aligned} \tag{5}$$

Here, ρ_s characterizes the spatial coherence length of the partially coherent beam at the source plane. Using the quadratic approximation of the wave structure function, the second term on the right-hand side of Eq. (4) is obtained as[12]

$$\begin{aligned} &\big\langle\exp\big[\psi(r,z) + \psi^*(r',z)\big]\big\rangle \\ &\approx \exp\left(-\frac{|r-r'|^2}{\rho_0^2}\right) \\ &= \exp\left[-\frac{2r^2 - 2r^2\cos(\theta-\theta')}{\rho_0^2}\right]. \end{aligned} \tag{6}$$

where the asterisk (*) denotes complex conjugation. The parameter ρ_0 represents the coherence length of a spherical wave propagating through biologically turbulence, and it is computed as follows[19]

$$\rho_0 = \left[\frac{\pi^2}{3}k^2 L\int_0^\infty \kappa^3\,\Phi_\mu(\kappa)\,d\kappa\right]^{-1/2}. \tag{7}$$

The coherence length ρ_0 is obtained based on the tissue's power spectral density that is given as[22]

$$\begin{aligned} \Phi_\mu(\kappa) &= \left[\frac{S\,l_c^3\,\Gamma(D_f/2)}{\pi^{3/2}\,2^{(5-D_f)/2}\,(1+\kappa^2\,l_c^2)^{D_f/2}}\right] \\ &\quad\times\exp\left(-\frac{\kappa^2\,l_0^2}{8\,\ln 2}\right), \end{aligned} \tag{8}$$

where S refers to the strength coefficient of the refractive-index fluctuations, κ denotes the spatial frequency, $\Gamma(\cdot)$ is the Gamma function, l_c is the correlation length, l_0 denotes the inner (small-scale) length parameter, and D_f corresponds to the fractal dimension characterizing the tissue structure.

By substituting Eq. (8) into Eq.(7) and performing the integration, the coherence length is obtained as follows[20]:

$$\begin{aligned} \rho_0 &= \left[\frac{\sqrt{\pi}}{3}k^2 L\,\Gamma\left(\frac{D_f}{2}\right)\frac{S}{2^{\frac{(7-D_f)}{2}}\,l_c}\right. \\ &\quad\left.\times\,U\left(2;\frac{6-D_f}{2};\frac{l_0^2}{8\ln 2\,l_c^2}\right)\right]^{-\frac{1}{2}}, \end{aligned} \tag{9}$$

where $U(\cdot)$ refers to the confluent hypergeometric function of the second kind. During propagation through turbulent biological tissues, beam energy is redistributed across various OAM modes owing to fluctuations in the turbulent refractive index, leading to the generation of OAM crosstalk.

The complex amplitude of the PCPO vortex beams transmitted through turbulent biological tissues can be expressed as the superposition of an infinite series of helical harmonic fundamental modes[12]:

$$E(r,z) = \frac{1}{\sqrt{2\pi}}\sum_{n=-\infty}^{+\infty} a_n(r,z)\exp(in\theta), \tag{10}$$

where the expression for the superposition coefficient $a_n(r,z)$ is given by

$$a_n(r,z) = \frac{1}{\sqrt{2\pi}}\int_0^{2\pi} E(\boldsymbol{r}',z)\exp(-in\theta)\,d\theta. \tag{11}$$

By performing the turbulence ensemble average of the above equation, the OAM probability density for the PCPO vortex beams can be derived as

$$\begin{aligned} \big\langle|a_n(r,z)|^2\big\rangle = \frac{1}{2\pi}\int_0^{2\pi}\int_0^{2\pi}\langle E(\boldsymbol{r},z)E^*(\boldsymbol{r},z)\rangle_{TS} \\ \exp\big[in(\theta-\theta')\big]\,d\theta\,d\theta'. \end{aligned} \tag{12}$$

By substituting Eq. (4) into Eq. (12) and utilizing the corresponding integral relation

$$\begin{aligned} \int_0^{2\pi}\exp[-im\phi_1 + \beta\cos(\phi_1-\phi_2)]d\phi_1 \\ = 2\pi\exp(-im\phi_2)I_m(\beta), \end{aligned} \tag{13}$$

the final expression for the OAM probability density of PCPO vortex beams in turbulent biological tissues is thereby obtained as

$$\begin{aligned} \big\langle|a_n(r,z)|^2\big\rangle &= i^{-2|n_0|}\frac{4\pi^2 k}{2-\gamma}\zeta\,[\rho(z)]^2 \\ &\quad\times(\delta\gamma z^{\frac{\gamma}{2}})^{\frac{2}{2-\gamma}}\exp\left(-\frac{2r^2}{\tilde{\rho}_0^2}\right) \\ &\quad\times\left|J_{n_0}\left[kr(\delta\gamma z^{\gamma-1})^{1/(2-\gamma)}\right]\right|^2 \\ &\quad\times I_{n_0-n}\left(\frac{2r^2}{\tilde{\rho}_0^2}\right). \end{aligned} \tag{14}$$

where $I_n(\cdot)$ represents the modified Bessel function of the first kind of order n, and $\tilde{\rho}_0$ is the effective spatial coherence length in turbulent biological tissues that can

©2026 The Author(s). This article is licensed under CC By 4.0

be given as

$$\tilde{\rho}_0 = \rho_0 \left(1 + \frac{\rho_0^2}{\rho_s^2}\right)^{-1/2}. \quad (15)$$

The integral of the OAM probability density over the radial extent of the receiving aperture R is the spiral harmonic energy at the receiving plane that corresponds to each OAM mode[12, 20]:

$$\Omega_n(z) = 2\pi \int_0^{\frac{R}{2}} \langle |a_n(r,z)|^2 \rangle \, r \, dr. \quad (16)$$

The ratio of the spiral harmonic energy of OAM mode n to the total spiral harmonic energy at the receiving plane defines the spiral phase spectrum of the OAM mode n of the PCPO vortex beams. This ratio can be expressed mathematically as[12, 20]

$$P(n|n_0) = \frac{\Omega_n(z)}{\sum_{i'} \Omega_{i'}(z)}. \quad (17)$$

Here, n_0 indicates the initial OAM mode index of the pin-like vortex beam, whereas n represents the analyzed OAM mode after passing through the turbulent biological tissue. The OAM probability $P(n)$ is calculated from the normalized modal spectrum, ensuring that each mode's contribution is divided by the total intensity for the probability normalization. The quantity $\sum_i \Omega_i(z)$ is computed numerically using the analytical model for each propagation distance z.

When $n = n_0$, $P(n \mid n_0)$ is the probability of correctly detecting the transmitted OAM mode n_0 at the receiving plane. Using the OAM mode transmission model for PCPO vortex beam transmission through turbulent biological tissues, the channel capacity of the OAM link employing PCPO vortex beam transmission can be evaluated.

The channel capacity can be computed as follows [12]:

$$\begin{aligned} C &= \max\left[H(n_0) - H(n_0|n)\right] \\ &= \max_{P(n_0)} \Big[-\sum_{n_0} P(n_0) \log P(n_0) \\ &\quad + \sum_n \sum_{n_0} P(n_0) P(n|n_0) \log \frac{P(n_0)P(n|n_0)}{\sum_{n_0} P(n_0)P(n|n_0)} \Big], \end{aligned} \quad (18)$$

where $H(n_0)$ is the entropy of the information source and $H(n_0 \mid n)$ is the conditional entropy given the received mode n. The number of channels is $N = n_i + 1$. $P(n_0)$, and the probability of emitting the OAM mode n_0 is $P(n_0)$. n_0 is the topological charge of the signal OAM mode, which varies from 0 to n_i.

3. NUMERICAL RESULTS AND DISCUSSIONS

Based on Eqs. Eq. (17) and Eq. (18), numerical calculations were performed to analyze OAM detection probability and channel capacity of the PCPO vortex beam propagated in turbulent biological tissues. The analysis utilizes the Rytov approximation, which is valid under weak refractive index fluctuations and scattering conditions. Given that biological tissues display minor refractive index variations, the selected values adhere to this weak-fluctuation regime, ensuring limited phase perturbations. This allows an accurate beam propagation description through the Rytov approximation, consistent with prior studies on weakly scattering biological media and the theoretical conditions necessary for such analysis [23]. The parameters were set as follows: $\lambda = 0.6328\mu$ m, $\gamma = 1.5$, $\omega_p = 1$, $C_p = 5.95$n m, $n_0 = 1$, and $\rho_s = 10\mu$ m, unless specified otherwise. The chosen tissue samples are the liver parenchyma (mouse), intestinal epithelium (mouse), upper dermis (human), and deep dermis (mouse) tissue types, the values for D_f are 2.60, 2.67, 2.67, and 2.72, the values for l_c are 10.24, 11.48, 5.24, and 5.29 μm, respectively, $S = 1 \times 10^{-4}$, $l_0 = 1.0$ μm , and $L = z$. In our simulation, upper dermis (human) tissue was used, and since the values of the phase modulation power parameter γ are 0.5, 1, and 1.5, we will suffice with studying the effect of γ with values 0.5 and 1.5, because 1 and 1.5 are close in their effect, but the effects of 0.5 and 1.5 are different [12].

Fig. 1 shows the spiral spectrum for PCPO vortex beams through turbulent biological tissues at $z = 50$ μm for different values of the OAM mode n with two different values of spatial coherence length parameter ρ_s and different phase modulation power γ. From this figure, it is evident that when $\gamma = 1$ and 1.5, the behavior of the spiral spectrum is identical when $n = n_0$ for two values of the spatial coherence length parameter $\rho_s = 1$ and 10, as shown in columns 1 and 2. However, in column 3, we notice the highest value of the spiral spectrum when $n = n_0 = 0$ and the spiral spectrum decreases as $n = n_0$ increases when $\gamma = 0.5$. Additionally, we find that as the spiral spectrum maxima when the detected mode index $n = n_0$, decreases for $n \neq n_0$. This is the classic signature of OAM crosstalk caused by scattering effects. The central peak shows the power that remains in the transmitted mode, while the symmetric sidebands ($n = n_0 \pm 1, n_0 \pm 2, \ldots$) reveal coupling into neighboring modes owing to tissue-induced phase perturbations. These sidebands directly indicate turbulence scrambling the helical phase $\exp(\check{}in_0\theta)$. The spectrum width reflects the crosstalk severity: a narrower spread indicates stronger OAM preservation. Effect of Spatial Coherence Length ρ_0: A larger source coherence length boosts the peak at n_0, showing how intrinsic coherence interacts with tissue turbulence. A highly coherent beam (large ρ_0) maintains a stable phase front, which helps prevent beam scattering. In this case, the effective coherence length $\tilde{\rho}_0 \approx \rho_0$, and turbulence dominated the degradation. For a low-coherence beam, $\tilde{\rho}_0$ becomes much smaller, meaning that the beam's own phase randomness amplifies turbulence effects, broadening the spectrum and reducing the main peak. Furthermore, it

©2026 The Author(s). This article is licensed under CC By 4.0

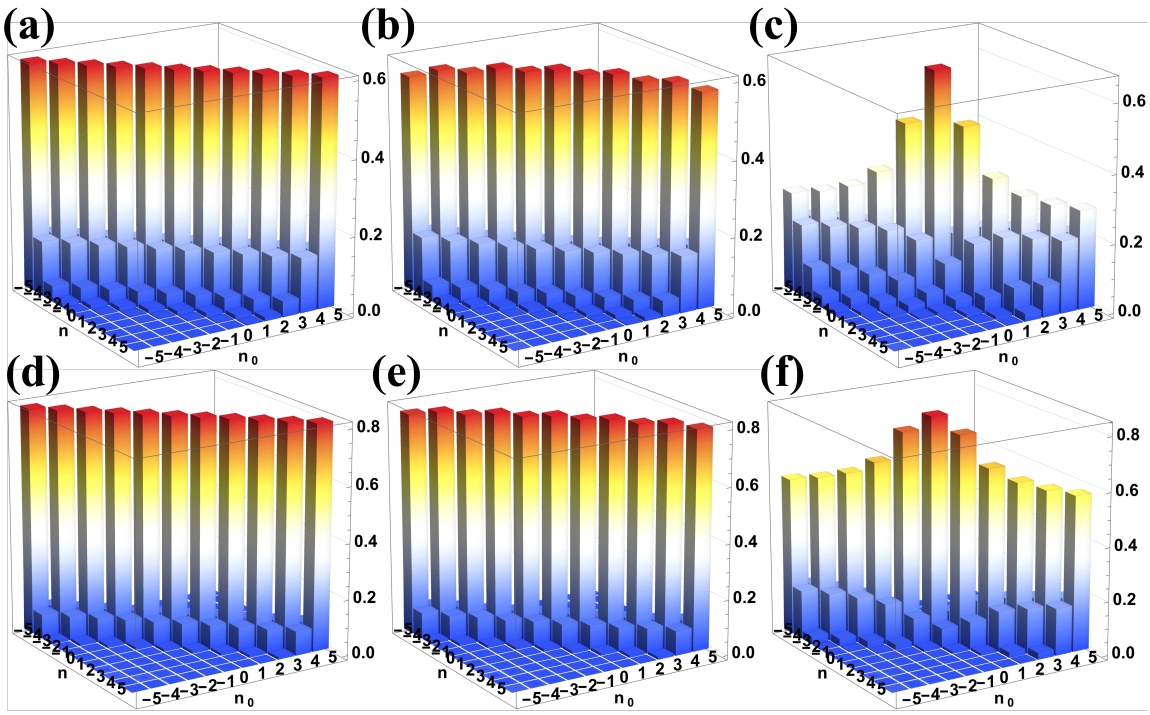


Figure 1. The spiral spectrum of PCPO vortex beams propagating through turbulent biological tissues at a depth of $z = 50$ μm is analyzed for the OAM mode n and three values of γ: (a, d) $\gamma = 1.5$, (b, e) $\gamma = 1$, and (c, f) $\gamma = 0.5$ at two different spatial coherence length parameter values: (a, b, c) $\rho_s = 1$ and (d, e, f) $\rho_s = 10$ μm.

can be inferred that, for dependence on the OAM mode n and the OAM mode number n_0, the spiral spectrum power increases for equal the OAM mode n and the OAM mode number n_0. While $n_0 \neq n$ usually spreads more and suffers greater distortion, pin-like beams behave differently. Its tightly localized profile makes $n_0 \neq n$ modes easier to blur by scattering, weakening their phase singularity early. $n_0 = n$ modes, with steeper phase gradients, initially resist these fine-scale distortions better, producing stronger detected power at short propagation ($z = 50$ μm). However, over longer distances, their larger effective aperture would likely make them more vulnerable.

Fig. 2, shows the distribution of the OAM detection probability of PCPO vortex beams through turbulent biological tissues against propagation distance with different values of the topological charge specifically at two of the phase modulation power parameter. From Fig. 2(a), We can see that the detection probability decreases more quickly for higher topological charges n_0 when $\gamma = 0.5$. This matches the standard image of OAM beams in turbulence. Higher n_0 modes have steeper phase gradients and larger ring diameters. In the tightly localized $\gamma = 0.5$ pin-like beam, a high n_0 vortex exerts a strong transverse phase curvature in a small region, making it extremely sensitive to small-scale perturbations. Tissue scatterers easily disrupt phase singularity and couple power into nearby modes. The larger effective diameter of high n_0 vortices also intercepts more inhomogeneities. Consequently, higher charges experience stronger turbulence-induced degradation, and the curves separate rapidly. Fig. 2(b), for $\gamma = 1.5$, detection probability is nearly independent of n_0, and all modes decay similarly. This emphasizes the advantage of the $\gamma = 1.5$ beam's Bessel-forming behavior. As it propagates, it approaches a pin-like structure composed of conical plane waves. Its non-diffracting, self-healing nature [24] provides all OAM orders with comparable robustness. Although a higher n_0 still implies a more complex phase, the extended, non-localized Bessel profile causes degradation to be dominated by cumulative, large-scale phase errors rather than mode-specific sensitivity. This causes the decay curves for different n_0 to converge and overlap. Therefore, the overall detection probability is higher for $\gamma = 1.5$ than for $\gamma = 0.5$ for all n_0. This reinforces the fact that the pin-like beam propagation state is inherently more resilient than the localized pin-like state. Its reduced susceptibility to diffraction and scattering preserves the integrity of the OAM more effectively, making it a superior choice for transmitting OAM modes through scattering tissues.

Fig. 3 shows the effect of the different spatial coherence lengths of partially coherent sources ρ_s on the OAM detection probability of PCPO vortex beams through turbulent biological tissues against propagation distance for two specific values for the phase modulation power parameter: a) $\gamma = 0.5$ and b) $\gamma = 1.5$. From this figure, it can be observed that for low spatial coherence ($\rho_s < 10\mu m$), increasing ρ_s strongly improves the OAM

©2026 The Author(s). This article is licensed under CC By 4.0

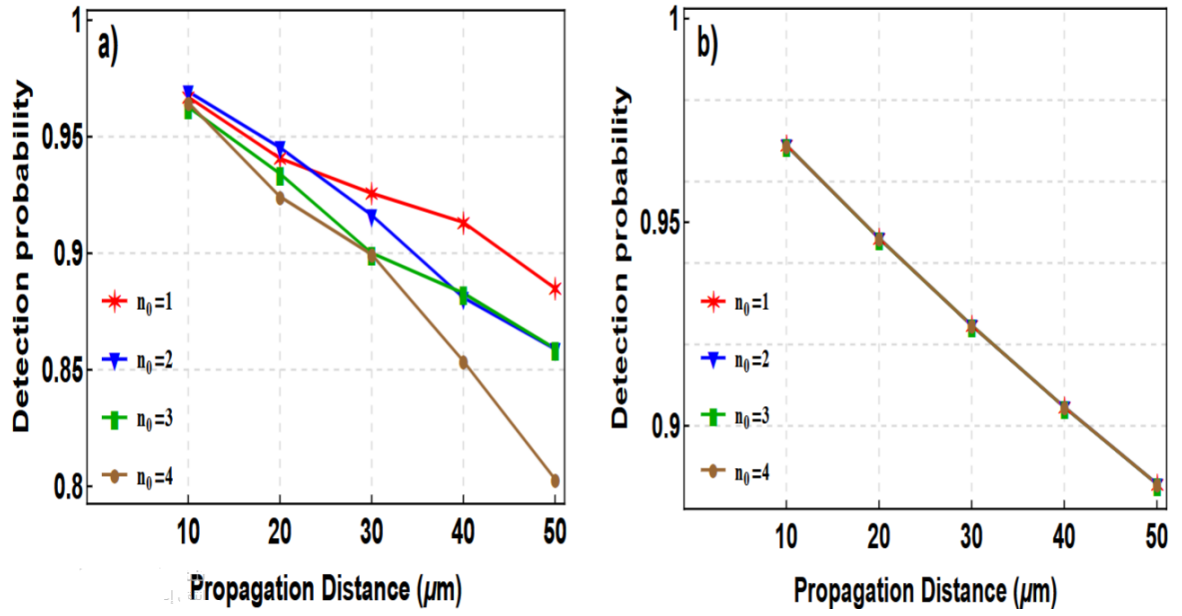


Figure 2. Detection probability of PCPO vortex beams through turbulent biological tissues against propagation distance for different values of the OAM mode number n_0, specifically at two γ values: a) $\gamma = 0.5$, and b) $\gamma = 1.5$.

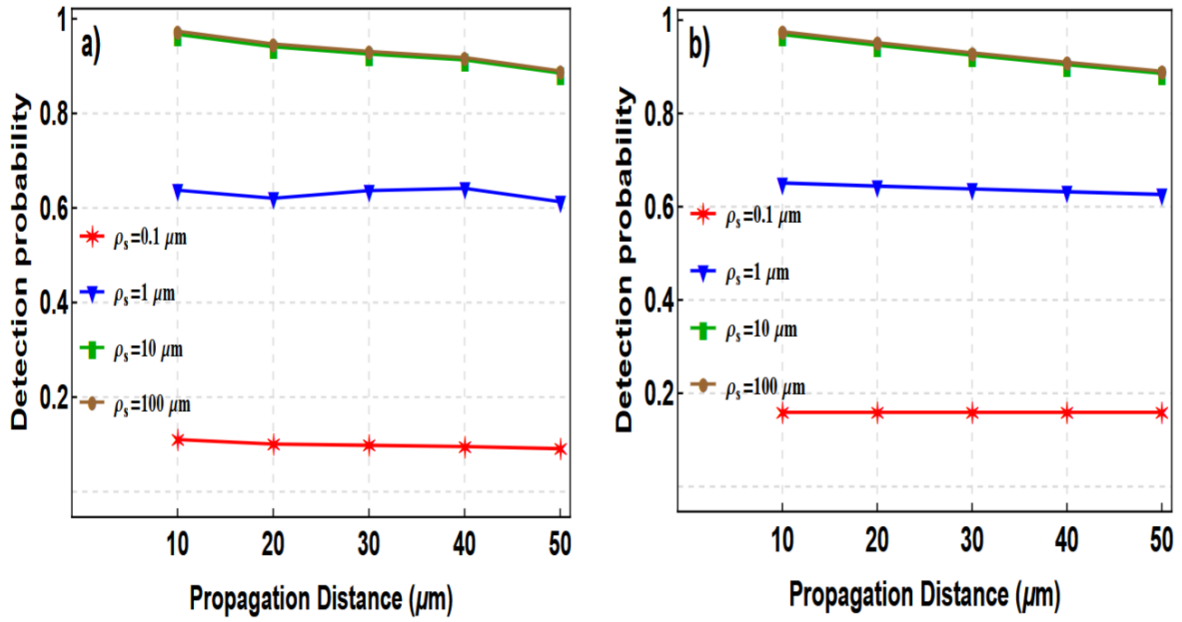


Figure 3. Detection probability of PCPO vortex beams through turbulent biological tissues against propagation distance for different values of the spatial coherence length ρ_s, specifically at two γ values: a) $\gamma = 0.5$, and b) $\gamma = 1.5$.

detection probability. This is because low-coherence beams have rapid phase fluctuations that partially shield them from turbulence ("coherence-induced resilience"), but this same randomness weakens the initial OAM structure. As ρ_s increases, the phase front becomes more ordered, allowing the vortex to form cleanly and boosting the detection probability until the beam is coherent enough to define its helical phase. The improvement is especially strong for $\gamma = 1.5$, because the Bessel-forming beam can exploit this growing coherence to establish its robust, non-diffracting profile. For high coherence ($\rho_s \geq 10\mu m$), increasing ρ_s gives n_0 further benefit, and the detection probability simply decays with distance. This peak marks the shift to a turbulence-limited regime in the flow. When $\rho_0 \gg 0$, the effective coherence length becomes $\tilde{\rho}_0 \approx 0$, indicating that the performance is capped by tissue turbulence rather than source quality. Beyond this threshold, the beam is already "fully coherent" for the channel, and boosting ρ_s cannot overcome the turbulence limit. Consequently, the curves for $\rho_s \geq 10$ μm overlap and follow the same decay dictated by the scattering strength. The performance gap between $\gamma = 0.5$ and $\gamma = 1.5$ is largest at low–intermediate coherence and shrinks at high ρ_s. At

©2026 The Author(s). This article is licensed under CC By 4.0

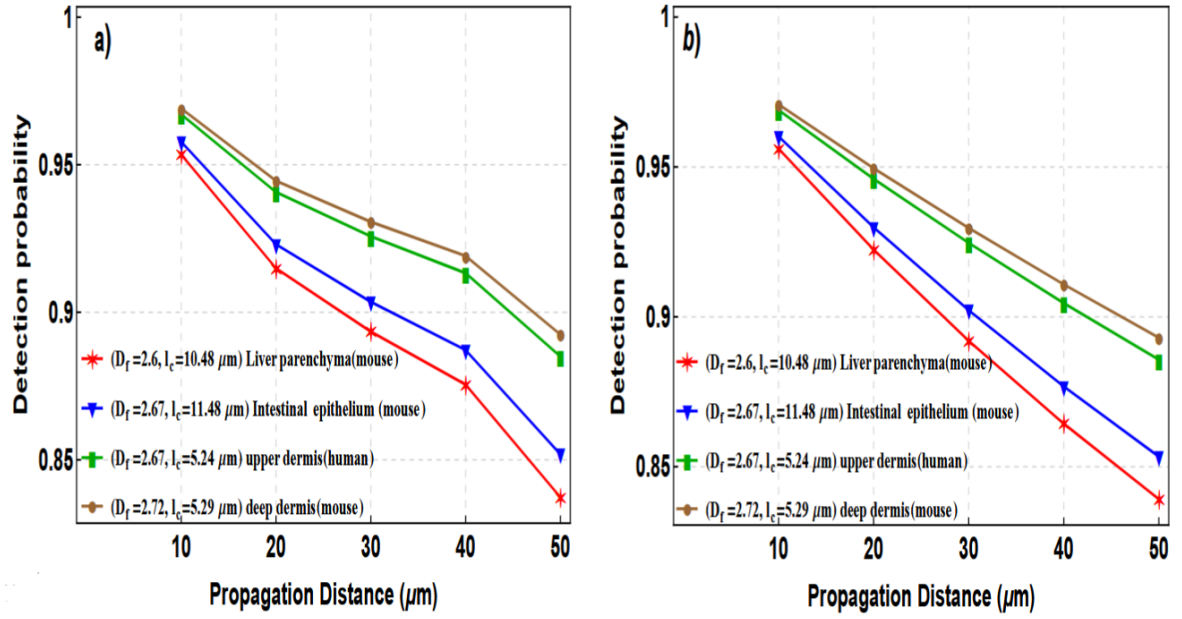


Figure 4. The detection probability of PCPO vortex beams propagating through turbulent biological tissues against propagation distance and different tissue(D_f and l_c) values, specifically at two γ values: a) $\gamma = 0.5$, and b) $\gamma = 1.5$.

low coherence, the internal structure of the beam is important: $\gamma = 1.5$ organizes partially coherent light into a more resilient Bessel-like form, outperforming the vulnerable pin-like $\gamma = 0.5$ beam. However, once the source provides a fully coherent wavefront, both beams enter the turbulence-limited regime, where degradation is governed mainly by ρ_0. The Bessel beam may retain a slight advantage, but its performance converges as external turbulence becomes the dominant constraint.

In Fig. 4 this study describes how the probability of detecting orbital angular momentum (OAM) in PCPO vortex beams changes as they propagate through turbulent biological tissues, considering different tissue (D_f and l_c) values and two specific values for the phase modulation power parameter: a) $\gamma = 0.5$, and b) $\gamma = 1.5$. Fig. 4(a) and (b) show OAM detection probability decreases with propagation distance z. The monotonic drop in the detection probability arises from cumulative scattering and wavefront distortion as the PCPO vortex beam travels through the tissue. The helical phase $\exp(\check{}in_0\theta)$ becomes increasingly perturbed, causing OAM crosstalk, where power leaks from n_0 into nearby modes. This is captured by the effective coherence length $\tilde{\rho}_0$, which decreases with the propagation distance $L = z$. A smaller $\tilde{\rho}_0$ enlarges the argument of the modified Bessel function I_{n_0-n}, broadening the spiral spectrum and reducing the retained power in mode n_0, thus lowering the detection probability. The detection probability is higher and declines more linearly for $\gamma = 1.5$ than for $\gamma = 0.5$. The contrast between the two γ-values reflects the impact of the phase modulation strength. For $\gamma = 1.5$, the beam rapidly evolved toward a Bessel-like profile, which is more resistant to diffraction and exhibits self-healing. This yields a smoother and more linear decline in the detection probability. For $\gamma = 0.5$, the beam remains pin-like for a longer duration. Although this provides high purity at very short distances, its tightly confined structure is highly vulnerable to scattering, resulting in a rapid nonlinear performance drop. Thus, γ controls the trade-off between short-range purity ($\gamma \approx 0.5$) and extended-range robustness ($\gamma \approx 1.5$). In addition, it can be inferred that the liver tissue yields the lowest detection probability, whereas the upper and deep dermis performs better. Tissue-dependent differences follow variations in the fractal dimension D_f and correlation length l_c. The liver's low D_f (2.60) and large l_c (10.24 μm) create more sizable correlated scattering structures that strongly distort the vortex phase front, enhancing OAM crosstalk. Dermal tissues, with smaller l_c (≈ 5.3 μm) and slightly higher D_f, contain finer, less correlated scatterers that behave more like random noise, producing a weaker coupling between modes. Across the tested parameter range, l_c is more influential than D_f, as the performance tracks closely with changes in the correlation length.

Fig. 5(a) and (b) show the detection probability of PCPO vortex beams as they propagate through turbulent biological tissues, taking into account different strength coefficients of the refractive-index fluctuations (S values) and two specific values for the phase modulation power parameter. From the Fig. 5(a), we can observe that detection probability decreases with increasing turbulence strength S for both γ values. Stronger turbulence directly amplifies the phase distortions because S scales the refractive-index fluctuation spectrum $\Phi_\mu(\kappa)$. As S increases, random phase disruptions become stronger and more frequent, shortening the spherical wave coherence length ρ_0 and therefore the effective coherence length $\tilde{\rho}_0$. Because $\tilde{\rho}_0$ governs the OAM crosstalk, a reduced

©2026 The Author(s). This article is licensed under CC By 4.0

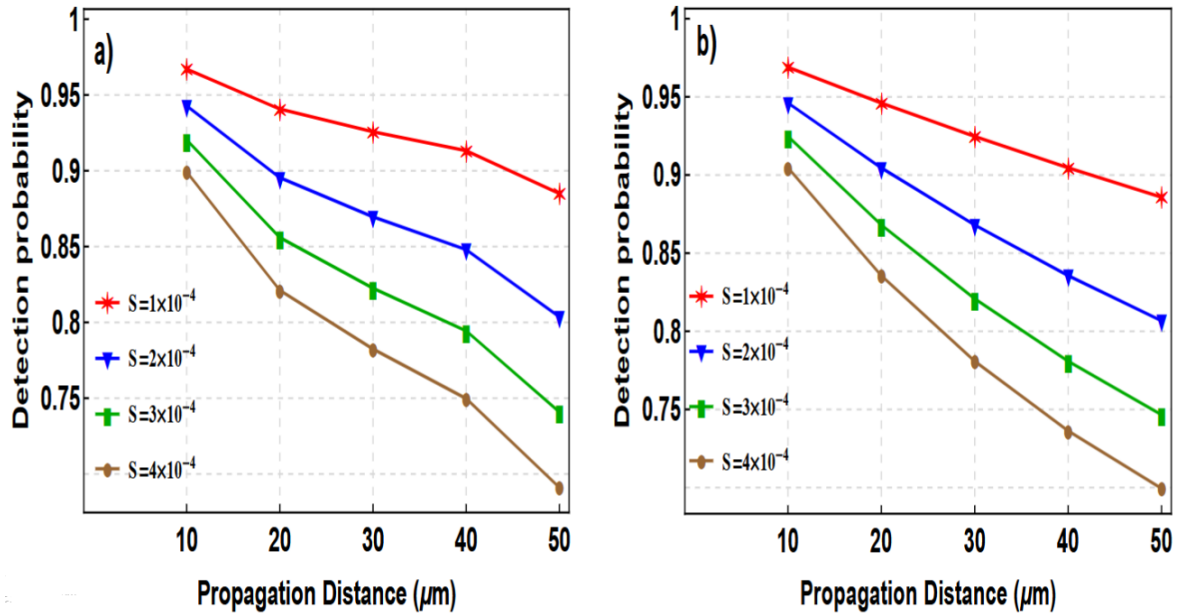


Figure 5. Detection probability of PCPO vortex beams through turbulent biological tissues against propagation distance for the different strength coefficients of the refractive-index fluctuations S values, specifically at two γ values: a) $\gamma = 0.5$, and b) $\gamma = 1.5$.

value accelerates the energy transfer from the transmitted mode n_0 into neighboring modes. Thus, a higher S intensifies scattering, scrambling the helical phase more quickly and sharply lowering the detection probability. Decay is non-linear and irregular for $\gamma = 0.5$ but more linear for $\gamma = 1.5$. The different decay shapes reflect the interaction of each beam structure with turbulence. When $\gamma = 0.5$, the beam remains tightly localized and pin-like, making it extremely sensitive to individual scattering events. Small-scale perturbations rapidly disrupt the narrow core and phase singularity, producing a steep and irregular decay as the vortex transitions abruptly into a scattered state. When $\gamma = 1.5$, this value drives the beam toward a Bessel-like profile, whose conical structure offers self-healing and better resistance to obstructions. Consequently, the detection probability decreases more smoothly and linearly as the beam degrades gradually rather than collapsing under the initial turbulence. Linearity indicates operation in a diffraction-resilient propagation regime. In this figure, it can be inferred that the highest detection probability for all S occurs at the shortest distance ($z = 10\mu m$). This reflects the cumulative nature of the OAM crosstalk. At $z = 10$ μm, the beam minimally interacts with the turbulent tissue; thus, scattering events and integrated phase distortions are still small. The detection probability is dominated by the initial beam quality and turbulence strength. The later portions of each curve reveal how rapidly each beam type (set by γ) deteriorates as scattering accumulates with depth.

The influences of small length-scale factor values l_0 along the propagation distances and on the detection probability of PCPO vortex beams through turbulent biological tissues are shown in Fig.6. By observing Fig. 6(a) and (b), it can be seen that the detection probability increases with the inner scale l_0. This result highlights how the beam interacts with the smallest refractive-index fluctuations of the tissue. The parameter l_0 sets the turbulence inner scale, cutting off high spatial-frequency components through the exponential factor $\exp(-\kappa^2 l_0^2/8\ln 2)$. These high-frequency fluctuations are the most damaging because they cause wide-angle scattering and rapidly break down the smooth helical phase of the vortex. As l_0 increases, these small-scale perturbations are suppressed, increasing the turbulence coherence length ρ_0 and thereby the effective coherence length $\tilde{\rho}_0 \sim 0$. A larger$\tilde{\rho}_0 \sim 0$ reduces the OAM crosstalk and improves the detection probability. Physically, a larger l_0 implies a smoother scattering environment. The effect of increasing l_0 is stronger for $\gamma = 0.5$ than for $\gamma = 1.5$. This behavior reflects the response of the spatial structure of each beam to small turbulence. The pin-like beam ($\gamma = 0.5$) has a tight, Gaussian-like center that is extremely sensitive to small-scale scattering effects; when l_0 is small, it degrades rapidly. Increasing l_0 removes these damaging high-frequency perturbations and produces a large improvement in stability. The Pin-Like beam ($\gamma = 1.5$) is already resilient owing to its extended self-healing structure. It still benefits from a larger l_0, but the relative gain is smaller because it is less dependent on suppressing small-scale turbulence. From this figure, it can be inferred that at a large l_0 (e.g., 4 μm), the detection probabilities for $\gamma = 0.5$ and $\gamma = 1.5$ converge. This key result shows that once the small-scale scatterers are filtered out, the remaining distortions arise from larger-scale tissue structures that affect both beam types in a similar manner. In this regime, cumulative low-frequency phase aberrations dominate, eliminating the advantages of one beam over the other. Thus, in tis-

©2026 The Author(s). This article is licensed under CC By 4.0

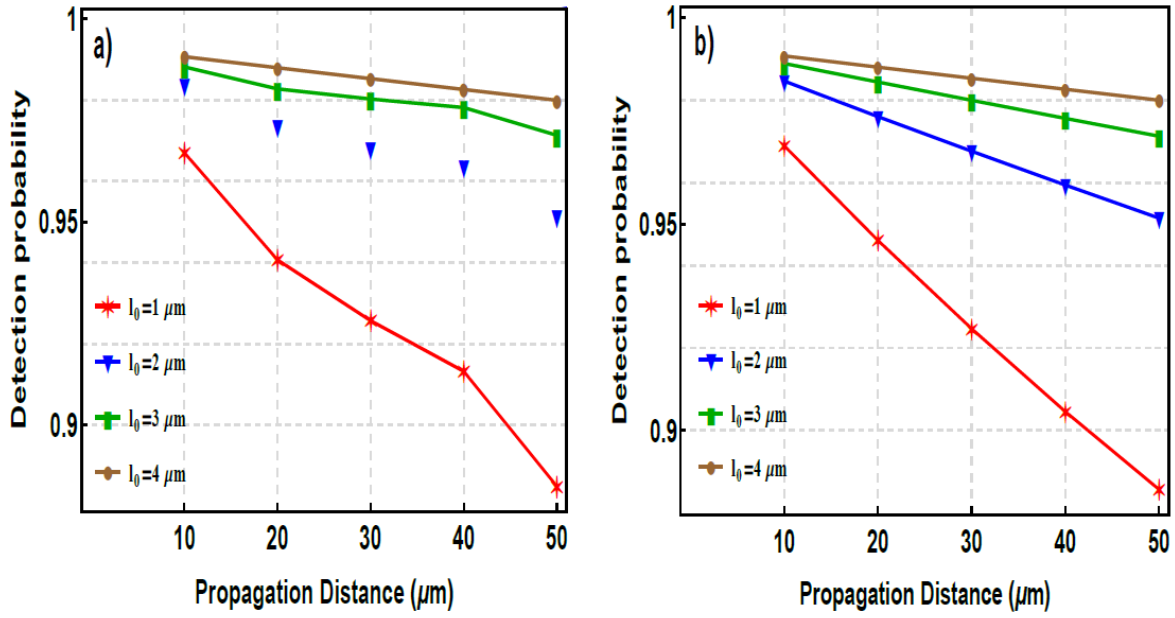


Figure 6. Detection probability of PCPO vortex beams through turbulent biological tissues against propagation distance for the different small length-scale factor values l_0 , specifically at two γ values: a) $\gamma = 0.5$, and b) $\gamma = 1.5$.

sues with large l_0, the beam choice becomes less critical, whereas in tissues with small, granular heterogeneity, the pin-like beam ($\gamma = 1.5$) provides a significant advantage.

Fig. 7(a) shows the effects of the propagation distance and strength coefficients of the refractive index fluctuations S values on channel capacity of PCPO vortex beams in the human upper dermis. From this figure, we can observe that the channel capacity decreases with increasing turbulence strength S and propagation distance z. Stronger turbulence or longer propagation increases the OAM crosstalk, broadening the conditional probability distribution $P(n \mid n_0)$. As this distribution becomes more uniform, the conditional entropy $H(n_0 \mid n)$ increases, reducing the mutual information and thus the channel capacity C. Physically, the system shifts from a regime of well-separated OAM modes to one in which all modes are mixed, driving the channel capacity toward zero as the distinguishability is lost. From Fig. 7(a) we can observe that for very strong turbulence ($S = 4$), channel capacity exhibits a brief non-monotonic rise before collapsing. This behavior likely reflects the early stage redistribution of power among the OAM modes. At very short distances, even under heavy turbulence, some power may momentarily concentrate in low-order modes, especially the robust $n = 0$ Gaussian-like component, making $P(n \mid n_0)$ slightly less uniform than expected and producing a small peak in the capacity. With further propagation, scattering fully randomizes the mode distribution, yielding an almost uniform $P(n \mid n_0)$. In this limit, the conditional entropy is maximized, and the channel capacity drops to zero, indicating the total loss of usable information. From Fig. 7(b) we can observe that Channel capacity increases with the small length-scale factor l_0. A larger inner scale suppresses high-frequency refractive-index fluctuations, which are the most effective at generating large-angle scattering and OAM crosstalk. This raises the turbulence coherence length ρ_0, yielding a narrower spiral spectrum and a more diagonal conditional probability matrix $P(n \mid n_0)$. Reduced conditional entropy $H(n_0 \mid n)$ leads directly to a higher channel capacity. Thus, tissues with larger l_0, that is, smoother microscopic structures, provide a fundamentally higher capacity OAM communication channel.

Fig. 8 shows the channel capacity of PCPO vortex beams in human upper dermis tissue along propagation distances for different values of the spatial coherence length ρ_s. In Fig. 8 (a) and (b), it is observed that at very low spatial coherence ($\rho_s = 0.1\mu m$), channel capacity is low and stays constant with distance. This plateau reflects a source-limited regime that is dominated by intrinsic incoherence. With such a small ρ_s, the beam is essentially an incoherent source carrying a vortex mask, and the OAM structure is already heavily degraded before entering the tissue. The resulting spiral spectrum $P(n \mid n_0)$ is broad from the start, and the effective coherence length $\tilde{\rho}_0 \approx \rho_s$ remains extremely small. Turbulence adds comparatively little degradation; therefore, the system remains stuck at its minimal coherence-limited capacity, regardless of the propagation distance. While for intermediate coherence ($\rho_s \sim 1-5, \mu m$), the capacity rises sharply but now decays with distance. In this transitional regime, the source coherence is sufficiently high for a clean OAM mode to form, boosting the initial capacity. However, ρ_s is still comparable to the turbulence coherence length ρ_0; therefore, both the source and tissue influence $\tilde{\rho}_0$. As the beam propagates, turbulence increasingly distorts the initially well-defined OAM mode, causing a distance-dependent decay in the ca-

©2026 The Author(s). This article is licensed under CC By 4.0

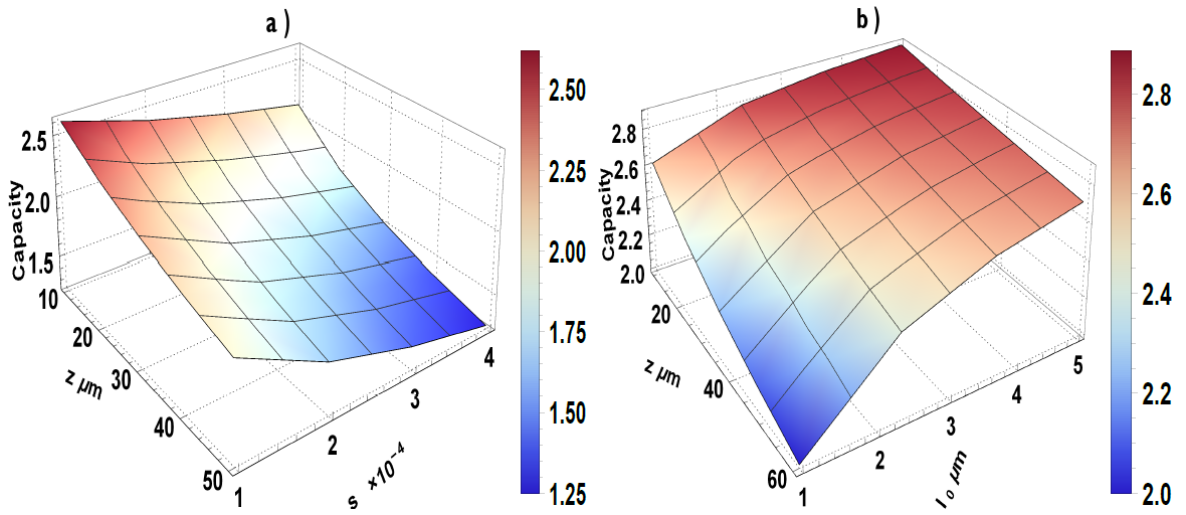


Figure 7. (a) Channel capacity versus the propagation distance for the different strength coefficients of the refractive index fluctuations$S$ values. (b) Channel capacity versus the propagation distance for different small length-scale factor values l_0.

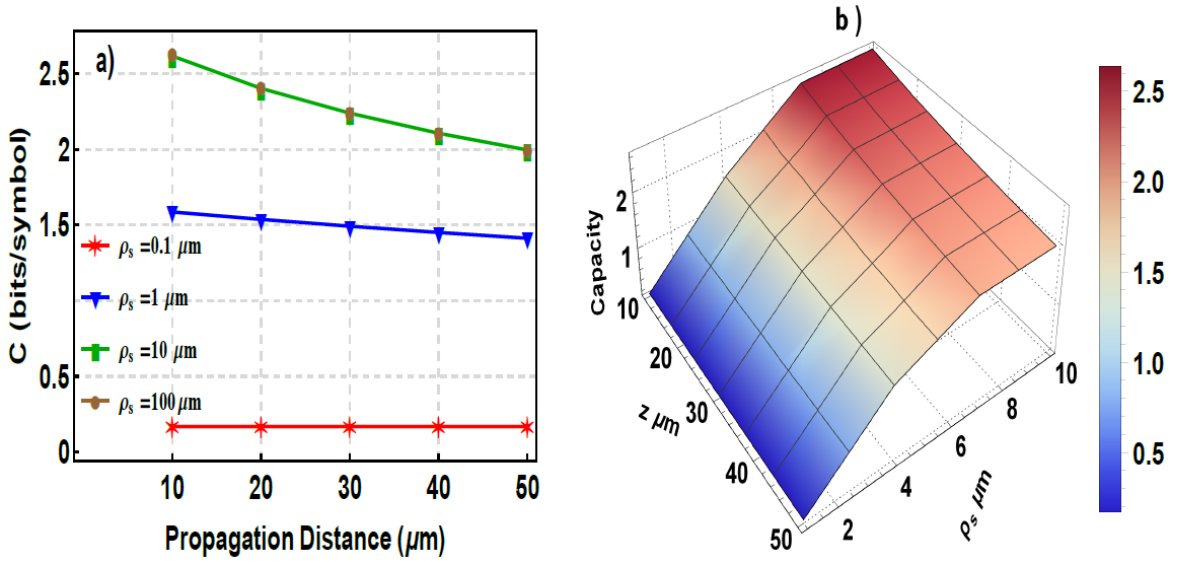


Figure 8. (a) and (b) Channel capacity versus the propagation distance for different values of the spatial coherence length ρ_s.

pacity. Here, the system reflects a balance between the OAM order and tissue-induced disorder. For high coherence ($\rho_s \geq 10\mu m$), the capacity saturates, and further increases in ρ_s offer no improvement; the capacity decays with distance. This marks the turbulence-limited regime of the flow. When $\rho_s \gg \rho_0$, the effective coherence becomes $\tilde{\rho}_0 \approx \rho_0$, meaning that turbulence, not the source, sets the performance ceiling. Therefore, the channel capacity is at its maximum possible value for that tissue environment, and any remaining decline with distance stems solely from cumulative scattering that reduces ρ_0, increases crosstalk, and lowers capacity. Further boosting the source coherence cannot overcome this turbulence-imposed limit.

Fig. 9(a) and (b) shows the channel capacity increases when the tissue correlation length l_c is small. The correlation length determines the size of the refractive-index inhomogeneities. A large l_c (as in liver tissue) corresponds to sizable, organized structures that impose correlated phase distortions across wide regions of the beam, efficiently couples power between OAM modes, and creates strong crosstalk. A small l_c (as in the upper dermis) corresponds to a finer, more random microstructure. These uncorrelated perturbations behave like noise rather than coherent phase screens, producing a weaker OAM mode mixing. This yields a longer turbulence coherence length ρ_0, and therefore a higher channel capacity. The channel capacity increases with a larger fractal dimension D_f. The fractal dimension measures the small-scale structural complexity. A higher D_f indicates a more irregular and space-filling tissue architecture. Although intuitively "rougher" tissue might seem to scatter more, a high D_f steepens the high-frequency roll-off in the turbulence spectrum $\Phi_\mu(\kappa)$, suppressing

©2026 The Author(s). This article is licensed under CC By 4.0

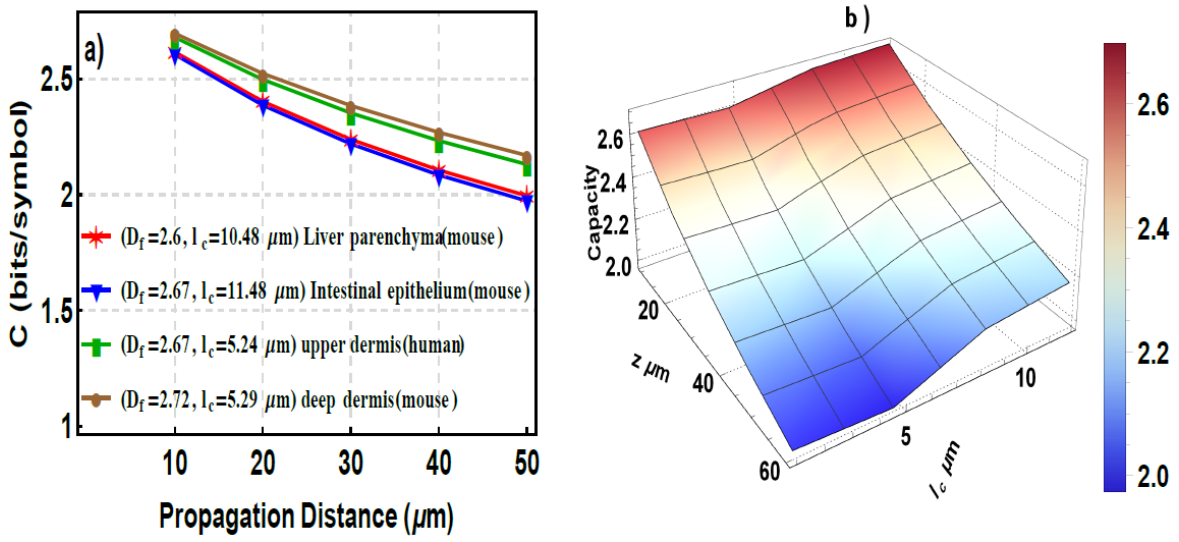


Figure 9. (a) and (b) Channel capacity versus the propagation distance for different tissue (D_f and l_c) values.

the very fine-scale scattering components that are most harmful to a vortex's phase singularity. When paired with a small l_c, a highD_f describes a finely heterogeneous but uncorrelated medium that is less damaging to the OAM integrity than large, smooth, and correlated structures. However, the combination of a high D_f and low l_c (e.g., upper dermis) yields the highest channel capacity. This provides a biophysical basis for predicting the tissue performance as an OAM communication channel. Therefore, high-capacity tissues (e.g., upper dermis) have high disorder and low l_c, which minimizes correlated phase distortion and preserves OAM purity. However, low-capacity tissues (e.g., liver parenchyma) have lower D_f and larger structures, producing strong, coherent phase scrambling. These findings show that capacity depends not only on total scattering but also on the spatial statistics of the tissue, enabling a priori predictions for biomedical optical link design.

4. CONCLUSION

This study extensively investigated the spiral spectrum, detection probability, and channel capacity of a partially coherent pin-like optical (PCPO) vortex beam through turbulent biological tissues based on the Rytov approximation. Our study reveals how biological tissue turbulence affects the propagation of partially coherent vortex beams, highlighting the conditions that preserve their structural robustness and performance in biological optical environments. Our analysis reveals that optimal performance is achieved through a strategic triad of tunability: the spatial structure of the beam, its coherence, and the properties of the tissue. Crucially, we identify the phase modulation power ($\gamma = 1.5$) as a key enabler, triggering a Bessel-forming transition that confers "topological charge resilience," allowing high-order OAM modes to propagate with remarkably similar robustness. This unlocks the potential for high-capacity mode-division multiplexing (MDM). Furthermore, we decoded the channel capacity of the tissue, showing that it is governed by the spatial correlation of scattering structures, not just total scattering. Fine-grained, disordered tissues (high fractal dimension D_f and low correlation length l_c) paradoxically form superior channels. We also defined an optimal spatial coherence length beyond which no further capacity gains were possible. In conclusion, this study shifts the paradigm from simply transmitting light through tissue to intelligently engineering light to cooperate with the statistical properties of the tissue. The PCPO vortex beam emerges not only as a carrier of data but also as a reconfigurable and resilient information vector. These results pave the way for advanced optical technologies in deep-tissue sensing, high-resolution imaging, and secure communication systems within living organisms, where light must navigate the intricate and dynamic landscapes of biological turbulence.

Declarations

- Funding
  No funding was received from any organization for this study.
- Conflict of interest/Competing interests
  The authors have no financial or proprietary interest in any material discussed in this article.
- Ethics approval and consent to participate
  Informed consent was obtained from all the participants.
- Consent for publication
  The authors confirm that informed consent was obtained for the publication of the data contained in this article.
- Data availability
  The research data are not available.
- Materials availability

©2026 The Author(s). This article is licensed under CC By 4.0

No materials were used in the present study.

- Code availability
  No code was used in the present study.
- Author contribution
  W.A.A.-B. contributed to the conceptualization and development of the theoretical model for partially coherent pin-like vortex beams in turbulent biological tissues, carried out the analytical derivations, wrote the original manuscript draft, and performed numerical simulations and data analysis. H.T.A.-A. conceived the research idea on pin-like OAM beams in turbulent biological tissue and verified the interpretation of the results. M.S.Q. contributed to the validation, visualization, and interpretation of the results. A.A.A. supervised the research, reviewed and edited the manuscript, and managed overall research. All the authors have reviewed and approved the final manuscript.

Acknowledgements

The authors acknowledge the use of Mathematica for numerical simulations, analytical computations, and figure preparation; LaTeX for manuscript preparation; and ChatGPT and Grammarly for language refinement.

REFERENCES

[1] H. O. Al-Nadary, A. A. Alkelly, M. A. H. Khaled, and L. F. Hassan, "The effective beam width of a partially coherent rectangular multi-gaussian schell-model vortex beam propagating in a turbulent plasma," *Sana'a Univ. J. Appl. Sci. Technol.*, vol. 1, no. 3, 2023.

[2] L. F. Hassan, A. A. Alkelly, and M. A. H. Khaled, "Polarization and coherence properties of a partially coherent elegant laguerre–gaussian vortex beam in turbulent plasma," *J. Appl. Phys.*, vol. 135, no. 19, 2024.

[3] M. S. Qusailah, A. A. Alkelly, and W. A. Al-Bahry, "The propagation properties of a lorentz–gauss vortex beam in a gradient-index medium," *Int. J. Opt.*, vol. 2023, no. 1, p. 3 772 408, 2023.

[4] F. M. Thabit, A. A. AlKelly, and M. A. Shukri, "Propagation of fully and partially coherent flat-topped multi-gaussian beams through axicons," *J. Opt. Soc. Am. A*, vol. 37, no. 5, pp. 759–767, 2020.

[5] X. Wang, M. Chen, Q. Yuan, L. Wang, and S. Zhao, "Transmission characteristics of partially coherent pin-like optical vortex beams in oceanic turbulence," *Phys. Scripta*, vol. 99, no. 6, p. 065 550, 2024.

[6] M. Cheng, L. Guo, J. Li, Q. Huang, Q. Cheng, and D. Zhang, "Propagation of an optical vortex carried by a partially coherent laguerre–gaussian beam in turbulent ocean," *Appl. Opt.*, vol. 55, no. 17, pp. 4642–4648, 2016.

[7] J. E. Morris, M. Mazilu, J. Baumgartl, T. Čižmár, and K. Dholakia, "Propagation characteristics of airy beams: Dependence upon spatial coherence and wavelength," *Opt. Express*, vol. 17, no. 15, pp. 13 236–13 245, 2009.

[8] Y. Ni, Y. Zhou, G. Zhou, and R. Chen, "Characteristics of partially coherent circular flattened gaussian vortex beams in turbulent biological tissues," *Appl. Sci.*, vol. 9, no. 5, p. 969, 2019.

[9] S. Altay Arpali and Y. Baykal, "Propagation of higher-order annular gaussian beams in biological tissues," *J. Opt. Soc. Am. A*, vol. 42, no. 8, pp. 1174–1181, 2025.

[10] M. Luo, Q. Chen, L. Hua, and D. Zhao, "Propagation of stochastic electromagnetic vortex beams through the turbulent biological tissues," *Phys. Lett. A*, vol. 378, no. 3, pp. 308–314, 2014.

[11] A. A. A. Ebrahim and A. Belafhal, "Effect of the turbulent biological tissues on the propagation properties of coherent laguerre–gaussian beams," *Opt. Quantum Electron.*, vol. 53, no. 4, p. 179, 2021.

[12] Y. Wu, Y. Zhang, Q. Wang, and Z. Hu, "Average intensity and spreading of partially coherent model beams propagating in a turbulent biological tissue," *J. Quant. Spectrosc. Radiat. Transf.*, vol. 184, pp. 308–315, 2016.

[13] D. Bongiovanni et al., "Free-space realization of tunable pin-like optical vortex beams," *Photonics Res.*, vol. 9, no. 7, pp. 1204–1212, 2021.

[14] J. Cao, L. Han, H. Liang, G. Wu, and X. Pang, "Orbital angular momentum spectrum of pin-like optical vortex beams in turbulent atmosphere," *J. Opt. Soc. Am. A*, vol. 39, no. 8, pp. 1414–1419, 2022.

[15] L. C. Andrews and R. L. Phillips, *Laser beam propagation through random media*, 2005.

[16] F. Saad and A. Belafhal, "A theoretical investigation on the propagation properties of hollow gaussian beams passing through turbulent biological tissues," *Optik*, vol. 141, pp. 72–82, 2017.

[17] C. Liu et al., "Robust transmission of pin-like vortex beams in plasma sheath turbulence," *Appl. Opt.*, vol. 64, no. 24, pp. 7076–7082, 2025.

[18] Z. Zhang et al., "Single-shot intensity-based measurement of high-order oam in partially coherent vortex beams," *Opt. Lasers Eng.*, vol. 193, p. 109 085, 2025.

[19] M. Lazrek, Z. Hricha, and A. Belafhal, "Propagation of partially coherent vortex hermite-cosine-hyperbolic-gaussian beams in turbulent atmosphere," *Opt. Quantum Electron.*, vol. 56, no. 10, p. 1631, 2024.

[20] F. Saad, A. A. A. Ebrahim, and A. Belafhal, "Spreading properties of a partially coherent modified anomalous vortex beam through biological tissues," *Opt. Quantum Electron.*, vol. 57, no. 5, p. 298, 2025.

[21] S. Chib and A. Belafhal, "Analyzing the spreading properties of vortex beam in turbulent biological tissues," *Opt. Quantum Electron.*, vol. 55, no. 1, p. 98, 2023.

[22] Q. Liang, B. Hu, Y. Zhang, Y. Zhu, S. Deng, and L. Yu, "Coupling efficiency of a partially coherent collimating laser from turbulent biological tissue to fiber," *Results Phys.*, vol. 13, p. 102 162, 2019.

[23] A. Yu and G. Wu, "Self-healing properties of optical pin beams," *J. Opt. Soc. Am. A*, vol. 40, no. 11, pp. 2078–2083, 2023.

[24] B. Wang and Z. Ding, "Simulation on scattering features of biological tissue based on generated refractive-index model," in *Journal of Physics: Conference Series*, vol. 277, 2011, p. 012 036.

©2026 The Author(s). This article is licensed under CC By 4.0